Published in final edited form as:
Mol Imaging Biol. 2013 December ; 15(6): . doi:10.1007/s11307-013-0653-8.

MR signal amplification for imaging of the mutant EGF receptor in orthotopic human glioma model

Mohammed Salman Shazeeb[1], **Suresh Gupta**[1], and **Alexei Bogdanov Jr**[1,2,#]

[1]Department of Radiology, University of Massachusetts Medical School, 55 Lake Ave North, Worcester MA 01655

[2]Department of Cell Biology, University of Massachusetts Medical School, 55 Lake Ave North, Worcester MA 01655

Abstract

Purpose—To investigate the potential of targeted MR signal amplification strategy for imaging of EGF receptor variant III (EGFRvIII) overexpression associated with the infiltrating margin of aggressive orthotopic brain tumors.

Procedures—F(ab')$_2$ fragments of humanized anti-EGFRvIII monoclonal antibody (EMD72000) were linked to deglycosylated horseradish peroxidase (HRP) and glucose oxidase (GOX). Detection of the F(ab')$_2$ conjugate pair colocalization *in vivo* was enabled by a subsequent IV injection of a low molecular weight paramagnetic substrate of HRP, diTyr-GdDTPA.

Results—The delivery of the targeted fragments to the tumor was validated using SPECT/CT imaging of radiolabeled anti-EGFRvIII F(ab')$_2$ conjugates. Further, by using 3T MRI, we observed time-dependent differences in tumor signal intensity and signal retention at the endpoint depending on whether or not the animals were pre-injected with the anti-EGFRvIII F(ab')$_2$ conjugates.

Conclusions—Imaging of EGFRvIII expression *in vivo* was enabled by consecutive administration of targeted F(ab')$_2$ conjugates and a paramagnetic substrate resulting in a tumor-specific receptor detection with high specificity and resolution.

Keywords

MRI; Molecular imaging; EGFRvIII; glioma; animal model; antibody fragment

Introduction

In recent years, improvements in imaging modalities such as CT and MRI have allowed earlier detection of astrocytomas. However, better prognostic indicators are required to allow stratification of patients so that individualized therapies can be implemented, evaluated, and optimized [1, 2]. Glioblastoma multiforme (GBM, grade 4 astrocytoma) is a primary brain tumor in adults characterized by uniformly poor outcomes. Molecular expression analysis shows that the expression of epidermal growth factor receptor (EGFR) alongside with cancer stem-cell signatures points to chemo/radioresistance in a large fraction (35-75%) of GBM cases [3].

[#]Corresponding author: Departments of Radiology and Cell Biology, University of Massachusetts Medical School 55 Lake Ave North, Worcester MA 01655 Tel.508-856-5571 FAX 508-856-1860 Alexei.Bogdanov@umassmed.edu.

The wild-type EGFR undergoes ligand-dependent dimerization followed by autophosphorylation of the EGFR dimer leading to downstream proliferative and anti-apoptotic signaling in cancer cells [4]. The most common EGFR mutant, EGFRvIII, is a constitutively expressed truncated variant of EGFR found in 24% to 67% of GBMs, and is a hallmark of especially aggressive gliomas [5, 6]. Within this subgroup of glioma patients, expression of EGFRvIII can be used as an independent predictor of disease burden and mortality [7, 8]). Since EGFRvIII receptor variant is not present in normal neurons and astrocytes, EGFRvIII is an ideal candidate biomarker for targeted diagnostic [9] and therapeutic applications. In anticipation of such applications, several monoclonal antibodies (mAbs) have been developed to specifically target the N-terminal extracellular domain III of EGFR (e.g. mAb L8A4 [9], mAb 806 [10, 11] and mAb 3C10 [12]). Administration of these antibodies resulted in reduction of EGFRvIII auto-phosphorylation and abrogation of downstream anti-apoptotic effects [10] consistent with the inhibition of EGFR receptor dimerization and/or EGF binding [13-15].

A humanized EGFR monoclonal antibody (mAb EMD72000) binds to antigenic epitopes on EGFRvIII which are distinct from epitopes of wild-type EGFR recognized by mAb C225 (cetuximab) [16]. We translated this observation into *in vivo* EGFRvIII specific antibody-mediated delivery of enzymes to tumors [17]. The receptor-targeted delivery of antibodies was followed by administering small molecule paramagnetic [18, 19] or a radioactive [20] substrates of peroxidase (Fig. 1). These imaging substrates are converted by the enzymes into reactive intermediates that bind to the receptor-expressing cells. The fact that the enzyme activities were required to be complemented (e.g. HRP and GOX pair) necessitates the co-localization of both enzymes at the target site in the tissue. In the case of MR imaging, the accumulation of chelated Gd at the receptor expression site resulted in transient enhancement of receptor-positive tumors on T1-weighted MR images.

We recently established that U87 glioma cells overexpressing EGFRvIII exhibit a glial phenotype and form infiltrating margins if implanted in the presence of vascular endothelial growth factor (VEGF) and basic fibroblast growth factor (bFGF) supplemented Matrigel providing a more accurate small animal model of GBM [21]. In this study, we performed a detailed investigation of MR imaging signatures of EGFRvIII receptor overexpression in U87ΔEGFR tumors using anti-EGFRvIII $F(ab')_2$ conjugates with deglycosylated MR-signal amplifying enzymes.

Materials and Methods

Synthesis of DTPA bis-tyramide

Bis-tyramide of DTPA was synthesized with 60% yield as previously described [19]. The product was analyzed using ^1H NMR and mass-spectrometry (FAB-MS, m/e: found: 632 $[M+H]^+$, theory 631.29). The gadolinium salt of DTPA bis-tyramide (diTyr-GdDTPA) was synthesized by combining diTyr-DTPA with a 1.5 molar excess of Gd_2O_3 in degassed, nitrogen-saturated water under argon for 72 h at room temperature. The solution was filtered through stacked glass fiber filters, and sterilized by filtering through a 0.1μm PES membrane (Millipore, Bedford MA). The purity of the product was verified by reversed-phase HPLC.

Synthesis of monoclonal antibody conjugates

Humanized anti-EGFRvIII antibody (EMD72000 mAb, Merck KGaA, Darmstadt, Germany) was dialyzed against 10 mM PBS, pH 7.5 before use and stored sterile-filtered. $F(ab')_2$ fragments of EMD72000 were prepared by digestion with pepsin (Sigma-Aldrich) using standard approaches. The intact antibody was removed on immobilized Protein A

chromatography and the fragments were purified using centrifugal filters (Amicon® Ultra-4), with a 50,000 MWCO membranes (Millipore). The modification of $F(ab')_2$ fragments with SANH (Thermo-Fisher Corp.) was performed in 0.1 M bicarbonate, pH 8 at the molar ratio of 4 mol SANH : 1 mol $F(ab')_2$ followed by purification on PD10 columns (GE Healthcare BioSciences Corp., Piscataway NJ) equilibrated with 0.1 M sodium acetate, pH 4.9. Protein concentrations of antibody/antibody fragments were measured using a Micro BCA assay kit (Thermo-Fisher Corp).

Deglycosylation of recombinant GOX (EMD Merck-Calbiochem) and HRP (Type IX, Sigma) was accomplished by treating 100 nmol of enzyme in 0.1 M sodium acetate, pH 5 with 10-molar excess of sodium periodate for 30 min. The reaction was stopped by adding 0.1 M glycerol and the enzymes were purified on PD10 spin-columns. The deglycosylation and blocking of the remaining aldehyde groups was accomplished by treating with 0.1 M hydroxylamine for 3 h. Deglycosylated GOX, in 0.1 M sodium bicarbonate pH 8 (25 nmol), was modified with C6-succinyl formylbenzoate (C6-SFB, Thermo-Fisher Corp.) at the molar ratio of 5 mol C6-SFB : 1 mol $F(ab')_2$ for 30 min and purified as described above. Deglycosylated HRP was modified with C6-SFB using a 10-fold molar excess of C6-SFB. The numbers of covalently conjugated 4-formylbenzoyl 4-hydraziniumnicotinate groups were determined as suggested by the manufacturer.

The conjugates 4-hydraziniumnicotinate-modified mAb $F(ab')_2$ fragment with C6-formylbenzoyl-modified enzymes were synthesized at the molar ratio of 1:2 ($F(ab')_2$: enzyme) in 0.1 M sodium acetate, 0.1% Tween-20, pH 4.9 for 4 h followed by adding 0.1 mM 2-hydrazinopyridine to stop the reaction. The obtained conjugates were purified using Superdex 200 columns (GE-Healthcare) in 0.1 M ammonium acetate, pH 7.0. The peaks positive for both mAb $F(ab')_2$ anti-EGFRvIII binding and enzymatic activity were collected and concentrated on Ultracel-50 membranes (Millipore, Billerica MA) and analyzed on 4-15% gradient SDS-PAGE. C225 mAb $F(ab')_2$ fragments conjugated to HRP and GOX used *in vitro* were prepared as described above.

Conjugation of MAG3 and ^{99m}Tc labeling EMD72000 mAb $F(ab')_2$-enzyme conjugates

To an aliquot of EMD72000 mAb $F(ab')_2$-HRP or EMD72000 mAb $F(ab')_2$-GOX in 0.1M HEPES buffer pH 8.0, fresh solution of NHS-MAG3 (5 mg/ml) in dry DMF was added drop-wise with agitation to a final MAG3/antibody molar ratio of 5:1. The reaction mixture was incubated at room temperature for 1 h, and then purified by Bio-spin P30 columns (Pierce Biotechnology, Rockford, IL) using 0.25 M ammonium acetate, pH 5.2 as eluent. Aliquots of 0.1 ml were dispensed and stored frozen at −20°C until used.

The radiolabeling of MAG3-linked $F(ab')_2$-GOX or $F(ab')_2$-HRP conjugates was performed following a procedure described in [22]. The labeled conjugates were purified using Bio-Spin P30 columns and the radiochemical purity was verified by using ITLC and gel-permeation chromatography.

In vitro cell culture experiments

U87ΔEGFR and U87-MG cells were grown in 10% FCS, RPMI1640. For *in vitro* MR imaging, U87-MG or U87ΔEGFR cells ($2{\cdot}10^6$ cells/sample) were incubated with HRP and GOX conjugated anti-EGFRvIII EMD72000 mAb $F(ab')_2$ or C225 (cetuximab, Merck KGaA) mAb $F(ab')_2$ (1 μg/ml total mAb fragment) followed by 0.15 mM of diTyr-GdDTPA substrate in 5 mM glucose/PBS pH 7.4, pelleted in 0.5 ml polypropylene tubes through a layer of 30% Histopaque-1077 (Sigma-Aldrich) in PBS and the pellets were subjected to MRI. Imaging was performed by using a T1-weighted spin-echo pulse sequence (TE 11 ms/TR 200 ms) on a 1.5 T Signa GE system with the use of a knee coil. Cell

viability was determined using the XTT assay (Roche). Titration data fitting and analysis were performed by using GraphPad's Prism4 software (La Jolla, CA).

Cell binding and internalization experiments

Adherent cells in 6-well plates (4 million cells/well) were incubated with EMD72000 mAb $F(ab')_2$-GOX/$F(ab')_2$-HRP conjugate mixture either at 4°C or at 37°C for 30 min. The specificity of binding was tested by using 4°C incubations with ^{99m}TcMAG3-labeled mAb $F(ab')_2$ conjugates either in the absence of, or in the presence of a 10-fold molar excess of unlabeled conjugates.

Internalization experiments were performed by using EMD72000 mAb $F(ab')_2$-HRP/ $F(ab')_2$-GOX conjugate mixture at 1:2 (w/w ratio). The bound conjugates were eluted by treating cells with 0.2 M glycine, pH 2.5 on ice for 15 min followed by neutralization with 1M Tris, pH 8.0. Internalized conjugates were extracted using 1.0% Igepal CA-630 in the presence of protease inhibitors. The amount of bound and internalized conjugates was determined by measuring the kinetics of HRP/GOX-coupled ABTS oxidation (Thermo-Fisher), in the presence of 5mM glucose. A mixture of HRP- and GOX- linked conjugates at 1:2 ratio (w/w) was used for calibration of the ABTS spectrophotometric assay.

Membrane protein extraction and immunoblotting

Cells at 50-75% confluency were harvested using TrypLE Express cell detachment solution (Invitrogen Corp. Carlsbad, CA). Cell membrane proteins were extracted using a CNM compartmental protein extraction kit (BioChain Institute Inc., Hayward, CA) and normalized per protein concentration using a Micro BCA Protein Assay kit (Thermo Scientific). The immunoblotting of protein-normalized lysates on PVDF membranes was performed by using anti-EGFR mAb (ab3103, AbCam, Cambridge MA) as primary antibody with subsequent digital imaging.

Animal model and *in vivo* imaging

All animal experiments and procedures were performed according to the guidelines approved by the Institute Animal Care and Use Committee (IACUC). An orthotopic human glioma xenograft model was prepared by stereotaxically implanting $5{\cdot}10^4$ U87ΔEGFR cells suspended in 3 μl of 10% Matrigel™ in serum-free RPMI containing 1 ng VEGF165 and 10 ng bFGF in the brain of athymic rats (Harlan, 150-200g, n=5). Cells were implanted under aseptic conditions (2.5 mm posterior to bregma, 2 mm lateral to midline, and depth of 3.5 mm) 12 d prior to first imaging session.

SPECT imaging

For *in vivo* imaging, 10-20μg of MAG3-$F(ab')_2$-GOX or MAG3-$F(ab')_2$-HRP were labeled with 1-2 mCi (37-74 MBq) ^{99m}Tc and administered via tail vein injection to U87 ΔEGFR tumor bearing rats. Nuclear images were acquired under isoflurane anesthesia at various time points (10min – 24h post IV injection) on a NanoSPECT instrument (Bioscan, Washington DC, USA) with computed tomography (CT) registration. InVivoScope 1.37 software (Bioscan) was used for CT and SPECT reconstruction, image fusion and calculation of imaging volumes.

MRI protocol and measurements

MRI experiments were performed on a Philips Achieva 3.0T/60 cm bore magnet equipped with 80mT/m actively shielded gradients. The animals were maintained at 37°C throughout the experiment and anesthetized using 1.5% isoflurane in a 30% oxygen/nitrogen mixture. A 26-gauge catheter capped with a needle port was placed in the tail vein for paramagnetic

substrate administration. A 45-mm-diameter, 30-mm-long birdcage RF coil was used for MR signal collection. Multi-slice T1-weighted MR images (TR/TE=700/8.2 ms) were acquired at various time-points with the following MRI parameters: slice thickness = 1.5 mm; slice separation = 0.15 mm; field-of-view = 25.6 mm × 25.6 mm; data acquisition matrix = 256 × 128, 4 NEX. Animals were imaged first on Day 1 (12 d after tumor cell implantation). A pre-contrast image was acquired followed by IV injection of 0.1 mmol/kg diTyr-GdDTPA and T1-weighted images were then acquired continuously over a 1.5-h period. On the next day (Day 2) the animals first received 100 μg of EMD72000 mAb $F(ab')_2$-HRP/$F(ab')_2$-GOX mixture at 1:2 (w/w ratio, 0.3 ml) by IV injection via the tail vein. Five hours later, a pre-contrast image was acquired followed by IV injection of 0.1 mmol/kg diTyr-GdDTPA and images were acquired over a 2-h period. On both days, pre-contrast T_2-weighted images were acquired to corroborate the presence of tumor observed in the T1-weighted slices.

Image analysis

Following IV infusion of diTyr-GdDTPA, the temporal evolution of the signal decay in the tumor was evaluated on Days 1 and 2. A region-of-interest (ROI) was drawn to circumscribe the entire contrast-enhanced region of the tumor visible at the first time-point collected after the contrast injection. The mean signal intensity value within the ROI was then calculated using ImageJ [23].

For each animal, the ROI signal intensity data from each selected tumor slice was plotted to generate a separate time-series plot for Day 1 (control, no $F(ab')_2$ conjugates) and Day 2 (with a pre-injection of $F(ab')_2$ conjugates). Due to differences in tumor size and growth heterogeneity, and variability in the exact contrast dose delivered from one animal to another, each signal-intensity time-point was normalized relative to the pre-contrast time-point for each slice:

$$S_{norm}(t) = \frac{S_{post}(t) - S_{pre}(0)}{S_{pre}(0)} \times 100 \quad \text{(Eq.1)}$$

where $S_{norm}(t)$ is the normalized signal intensity at time t, $S_{post}(t)$ is the signal intensity at time t, and $S_{pre}(0)$ is the signal intensity in the pre-contrast slice.

The normalized signal-decay plots for each brain slice were used to calculate decay time constants (DTCs) using a monoexponential and a biexponential decay model:

$$y_{monoexp}(t) = A_0 \cdot e^{-t/\tau_0} + offset \quad \text{(Eq.2)}$$

$$y_{biexp}(t) = A_1 \cdot e^{-t/\tau_1} + A_2 \cdot e^{-t/\tau_2} \quad \text{(Eq.3)}$$

where $y_{monoexp}(t)$ and $y_{biexp}(t)$ are the signal intensities at time t; and A_0, A_1, A_2 are the amplitudes of each signal-decay component; τ_0, τ_1, and τ_2 are the DTCs for the respective models.

For each animal, the normalized signal-decay plots of the tumor ROI for each brain slice from Day 1 and Day 2 were fitted with both models. Mean values for τ_0, τ_1, and τ_2 were obtained for each animal by averaging the DTCs of each ROI from all selected tumor slices of the same animal. The mean values for τ_0, τ_1, and τ_2 were calculated for each animal on Day 1 and on Day 2. Student's paired *t* test was performed on the overall average of the DTCs from all the animals to check for any significant differences between Day 1 and Day 2.

Histology

Following the MRI studies, animals were euthanized and their brains were removed and fixed in buffered 10% paraformaldehyde (Electron Microscopy Sciences). Paraffin-embedded sections (6 μm) were deparaffinized, treated with Retreivagen A (Pharmingen), pH 6 at 83°C for 20 min, washed with TBS/1mM EDTA, pH 8 at 65°C, for blocking endogenous phosphatase activity and blocked using 10% serum, 10 mg/ml BSA in TBS for 4 h. The sections were incubated with anti-EGFR mouse mAb (Abcam), or digoxigenin-labeled anti-HRP mAb (clone 2H11, Abcam, Cambridge MA) followed by anti-mouse alkaline-phosphatase (AP) linked antibodies or anti-digoxigenin $F(ab')_2$ conjugated with AP (Roche, Indianapolis IN) and BCIP/NBT (Roche). The sections were counterstained with Vector Nuclear Fast Red stain (Vector Laboratories, Burlingame CA) to contrast the nuclei.

Results

EGFRvIII expression and imaging *in vitro*

We subjected EMD72000 mAb to pepsin digestion and isolated $F(ab')_2$ to decrease both the size and the Fc receptor mediated uptake of the targeted $F(ab')_2$-enzyme conjugates *in vivo*. We then obtianed a confirmation that the levels of EGFRvIII expression in U87ΔEGFR cells were sufficient for anti-EGFRvIII binding detection: $F(ab')_2$ labeled with AlexaFluor AF488 stained cell spheroids and revealed a subfraction of highly migratory cells (Fig. 2b). Immunoblotting of cell membrane extract of wild-type U87-MG and U87ΔEGFR by using anti-EGFR mAb (ab3103), which reacts with both wild-type and truncated EGF receptor variants revealed a 150 kD band which was identified as EGF receptor. Unlike the parent U87-MG line, U87ΔEGFR cells expressed three major anti-EGFR reactive products with the majority (i.e. 65%) of anti-EGFR-reactive proteins represented by a lower molecular weight truncated EGFRvIII expression product (Fig. 2c).

The synthesis of EMD72000 mAb $F(ab')_2$ fragments and their conjugation with HRP and GOX required further testing for binding specificity *in vitro*. Both radiolabeled $F(ab')_2$-HRP and $F(ab')_2$-GOX showed highly specific association with U87ΔEGFR cells that could be inhibited by an excess of non-labeled antibody conjugates (Fig. 3a). The binding of $F(ab')_2$-HRP conjugates was more efficient than $F(ab')_2$-GOX conjugates suggesting a 2-fold higher amount of $F(ab')_2$-GOX for optimal complementation of enzyme activities that was monitored using peroxidase-mediated oxidation of ABTS substrate as a readout. The measurement of HRP-generated signal (which depended on complementing GOX-mediated oxidation of glucose) confirmed that EMD72000 mAb $F(ab')_2$ conjugate binding was 5 times greater in U87ΔEGFR cells than U87-MG, and that most of this binding (about 85%) was associated with the cell surface at 4°C. At 37°C, about 20% remained externalized on the cell surface while the remaining 80% of conjugates was internalized (Fig. 3b).

Because tumor detection *in vivo* using the amplification approach depends on the extent of antibody-enzyme mediated MR signal change, we determined whether anti-EGFRvIII-enzyme conjugates that remain exposed on the cell surface could generate a change in the MR signal. MR imaging was performed on U87-MG cells and U87ΔEGFR spheroids incubated in the presence of an optimized ratio of $(F(ab')_2$-HRP/$F(ab')_2$-GOX conjugates and then treated with cell impermeable diTyr-GdDTPA substrate (0.15 mM) dissolved in PBS containing glucose (0.5 mM). No MR signal changes were detected in the parent U87-MG cell line, whereas U87ΔEGFR cells showed a significant MR signal change as assessed on T1-weighted images (compare wells 1 and 3, Fig. 4a), suggesting that MR signal changes were specific to the mutant form of the receptor. Treatment of EGFRvIII-positive spheroids with anti-EGFRvIII (EMD72000) antibody conjugates resulted in 8-fold MR signal increase

over background (Fig. 4b), while there was no significant difference in receptor protein expression between mutant and wild-type EGFR expressing cells.

In vivo imaging experiments (SPECT/CT)

SPECT/CT imaging was performed to evaluate the uptake of EMD72000 mAb F(ab')$_2$ enzyme conjugates in U87ΔEGFR orthotopic xenografts using ^{99m}Tc-labeled tracer amounts of the conjugates (1 μg F(ab')$_2$ fragment conjugate/animal). Using a conjugate of EMD72000 F(ab')$_2$ with deglycosylated HRP we demonstrated that receptor-targeted conjugates showed a prominent binding to U87ΔEGFR tumors (Fig. 5a-d). The radioactivity accumulated in the tumor exceeded the radioactivity of contralateral brain 29 times (i.e. target-to-background ratio was 29:1) with the concentration of accumulated F(ab')$_2$-HRP radioactivity (measured in μCi/mm^3 of the tissue) in the tumor being only approximately 2-fold lower that in the liver and kidneys. The target-to-background ratio was even higher in the case of mAb F(ab')$_2$-GOX conjugate (40:1), however, the uptake in the liver was higher than that of tumor xenografts resulting in accumulated radioactivity concentration ratios of 1:3 (tumor/liver). By using volume analysis of time-dependent accumulation of ^{99m}Tc labeled conjugates in the tumor and heart vs. the whole-body radioactivity we determined that the half-life of the conjugates in the bloodstream was 2.58 ± 0.71 h whereas the half-life of tumor accumulation was 2.76 ± 0.40 h.

In vivo Magnetic Resonance Imaging and histology corroboration

We performed MR imaging to investigate paramagnetic-substrate (diTyr-GdDTPA)-mediated signal enhancement of U87ΔEGFR orthotopic human glioblastoma xenografts. On Day 1 diTyr-GdDTPA was administered and brain tumors were imaged immediately after injection. After diTyr-GdDTPA had been completely eliminated, a second experiment was conducted on Day 2 when the same animals were injected with EMD72000 mAb F(ab')$_2$-GOX/HRP 5 h before injecting diTyr-GdDTPA. Fig. 5e shows sequential T1-weighted MR images of the rat brain demonstrating U87ΔEGFR xenograft enhancement as a function of time post-IV injection of diTyr-GdDTPA. On both Days 1 and 2, the T1-weighted images showed strong initial enhancement of the tumor within minutes after IV diTyr-GdDTPA injection (Fig. 5e). This initial enhancement was significantly higher when diTyr-GdDTPA followed an injection of EMD72000 mAb F(ab')$_2$ conjugates (Fig. 5e: Day 2 – 7 min) than without corresponding conjugates injection (Fig. 5e: Day 1 – 7 min). The initial images on both days (i.e. in the presence as well as in the absence of EGFRvIII-targeted conjugate pre-injection) showed a homogeneous enhancement of the entire tumor region with no delineation between core and interface regions. However, at later time points, (40-60 min after diTyr-GdDTPA administration), a strong and differential enhancement of the tumor volume was observed with the margins of the tumor appearing brighter (Fig. 5e, Fig. 6b, inset). These areas of enhancement were matched to U87ΔEGFR tumor margins that showed a strong positive reaction with EMD72000 mAb F(ab')$_2$ (Fig. 6b). Multiple areas of tumor margins and tumor microdeposits that were easily identifiable with H&E stain (Fig. 6a) were reactive with the antibody against HRP (Fig. 6c).

As a part of the assessment of the efficacy of EGFR targeted imaging, kinetic analysis of the *in vivo* MR signal enhancement was performed. The relative percent change in T1-weighted signal intensity of tumor ROIs was significantly higher with EMD72000 mAb F(ab')$_2$-GOX/HRP administration (Day 2) as compared to without pre-injection (Day 1) at the initial time points (Fig. 5f). The signal-intensity-decay (SID) curves of diTyr-GdDTPA washout from tumor regions before conjugate injection (Day 1) and after EGFRvIII-targeted conjugate injection (Day 2) exhibited biexponential decay for both days; χ^2 analysis using an *F* test found a biexponential function ([Eq. 3]) to best model the SID curves for the tumor regions before and after injection of EGFRvIII-targeted conjugates (Day 1 and Day 2). Fig.

5g shows a comparison of the two separate decay time constants (DTCs) (short τ_1 and long τ_2) between Day 1 and Day 2 obtained from normalized T1-weighted SID curves in U87ΔEGFR tumors as a function of time post-diTyr-GdDTPA injection. Both the DTCs (τ_1 and τ_2) were significantly longer on Day 2 (12 ± 0.4 min and 122 ± 35 min, respectively) compared to Day 1 (6 ± 3 min and 81 ± 28 min, respectively) (Fig. 5g).

Discussion

The imaging of cell-surface receptors in tumors is usually accomplished by injecting radiolabeled antibodies or antibody fragments into the blood stream followed by a delay during which unbound antibody is cleared from the circulation. The latter step is critical for generating high signal to noise ratio (SNR) images since signal from circulating antibody distributed in blood plasma obscures the specific signal. Thus, the use of long-circulating antibodies is not conducive to PET imaging with isotopes having a short half-life [24]. This problem can be rectified by using smaller engineered diabodies that have two binding centers and the necessary avidity but a much lower molecular mass and shorter blood half-lives than IgGs [25, 26].

An alternative approach is to deliver the antibody or other target-specific molecule and the signal-generating molecule sequentially over time [27-29]. In this strategy, signal generating molecules can be recognized by bispecific antibodies [29]. Antibodies can also be modified with chemical moeties that bind to, or react with chemical groups of the signal generating chelated metal cations [30, 31]. We demonstrated the efficacy of this approach by conjugating a receptor-specific antibody to enzymes (HRP and GOX) which catalyzes the oxidation of a paramagnetic substrate leading to its retention and accumulation at the binding site of the tumor-targeted antibody-enzyme conjugates [20, 32]. In turn, the paramagnetic substrate functions as a reducer of oxidized peroxidase and restores its enzymatic activity so that the chemical reaction is not self-limiting. The benefit of this targeted enzyme imaging approach is in the specific signal that is generated only if both conjugates with complementing activities co-localize at the target site. Since non-specific accumulation antibodies in tumors lacking the target molecule is highly variable, the absence of the receptor target expression leads to much lower tumor-associated signals as demonstrated by us previously by using orthotopic implantation of Gli36ΔEGFR cells [17].

In this research we set out to test the receptor-targeted self-complementing enzymatic signal amplification system in an aggressive glioma model that exhibits a more typical morphology, i.e. in U87ΔEGFR gliomas, expressing a truncated EGFR variant (EGFRvIII). Using an antibody fragment of anti-EGFRvIII (EMD72000) we found that U87ΔEGFR cells express high levels of EGFRvIII (Fig. 2) and the binding of EMD72000 mAb F(ab')$_2$ conjugates to this receptor has high specificity as demonstrated in competitive inhibition studies (Fig. 3a). The binding affinity constants (K_D) of the intact EMD72000 and the Fab fragment of EMD72000 to EGFR have been reported as 1–10 nM and 113 ± 25 nM, respectively [33]. Since the F(ab')$_2$ fragments of EMD72000 (used in this study) have two binding sites compared to a single one in the Fab fragment, the K_D of F(ab')$_2$ fragments is expected to be lower than Fab fragments and similar to intact antibody indicating a higher binding affinity of F(ab')$_2$ fragments to EGFR. The enzymatic activities of HRP and GOX F(ab')$_2$-conjugates resulted in complementation that was detected by a high GOX-dependent HRP reaction rate in U87ΔEGFR cells (Fig. 3b) which was absent or much lower in cells expressing wild type EGFR (U87-MG cells) (Fig. 2c). Finally, we observed that although the majority of the conjugates were internalized after incubating with cells at 37°C, a significant fraction of conjugates (20%) still remained on the surface and were available for catalyzing oxidation of a circulating paramagnetic contrast agent, diTyr-GdDTPA, and thus mediating a receptor-dependent amplification of MR signal. To test this hypothesis we

incubated U87-MG and U87ΔEGFR cells in culture with diTyr-GdDTPA and found that a significant MR signal amplification was detectable on T1-weighted images within the following 2 hours (Fig. 4).

Furthermore, SPECT/CT imaging of radiolabeled EMD72000 mAb F(ab')$_2$-HRP or EMD72000 mAb F(ab')$_2$-GOX conjugates *in vivo* revealed the ability of both antibody conjugates to reach the tumor after IV administration (Fig. 5a-d). It is possible that prior deglycosylation of the enzymes linked to EMD72000 mAb F(ab')$_2$ fragments may have prolonged the circulation time of the antibody-enzyme conjugates and assisted in their accumulation at the site of the tumor due to a reduction in opsonization and/or binding of the conjugates to cell surface lectins. Our SPECT data also suggests the feasibility of subsequent MR imaging at 5 hours after the injection of the conjugates since: 1) at the time corresponding to two blood half-lives only low concentrations of the EMD72000 mAb F(ab')$_2$ conjugates should be expected in the blood; 2) the conjugates will be too diluted to result in the complementation of enzymatic activities and substrate oxidation in the blood.

MR imaging carried out following administration of diTyr-GdDTPA alone (Day 1 testing) or following pre-injection of animals with EMD72000 mAb F(ab')$_2$ conjugates (Day 2), showed a greater initial MR signal intensity enhancement of U87ΔEGFR tumors that were pre-treated with conjugates as compared to the same tumors before the injection of conjugates (Fig. 5e). These results demonstrate not only the utility of IV administered EGFRvIII-antibody fragments in targeting this highly malignant tumor type, but also the feasibility of modifying these antibody fragments so that they become capable of generating an amplified MR signal and detectible contrast on T1-weighted MR images, when administered with an appropriately functionalized paramagnetic contrast agent. As confirmed by histology, this pre-targeted MR amplification strategy was highly effective in demarcating the margins of EGFRvIII receptor expressing tumors (Fig. 6).

EGFRvIII-antibody pre-targeting also resulted in changes of the washout kinetics of the diTyr-GdDTPA mediated MR signal (Fig. 5f). The representative decay curve corresponding to the injection of contrast agent alone (crosses) starts at ~70% and decays to ~20% with reaching a plateau by the 80th minute. In contrast, the decay corresponding to the kinetic analysis performed in the same animal after the contrast agent was injected after the preinjection with targeted conjugates (circles) has not reached a plateau even after 110 min suggesting a longer retention time in the tumor. The decay fits for each curve clearly indicated statistically different decay time constants for both the fast and slow components as indicated in 5g. The decay time constants calculated from normalized MR signal intensities were used to compare diTyr-GdDTPA washout due to variation of tumor sizes studied on consecutive days. An overall increase in DTCs (τ_1 and τ_2) was observed when the tumor-bearing animals were pre-injected with specific targeted conjugates (Fig. 5g). The DTC analysis indicates longer retention of paramagnetic products by tumor cells on Day 2 consistent with the accumulation and retention of diTyr-GdDTPA as a result of the presence of the targeted HRP-GOX enzyme amplification pair, which was confirmed by comparing the morphology of tumor margin positive for receptor expression with the MRI appearance of the same brain area (Fig. 6b).

Signal intensity decay analysis measured in Gli36ΔEGFR-bearing rats in our previous study found the washout of diTyr-GdDTPA to be monoexponential throughout the tumor volume generating a single DTC (τ_0) on Day 1, which we attributed to the washout of free diTyr-GdDTPA. Pre-injection with antibody-conjugates in the same study resulted in a biexponential washout of diTyr-GdDTPA reflecting the presence of paramagnetic products at the EGFRvIII target sites where the substrate was converted by the enzymes. In our current study however, U87ΔEGFR gliomas exhibited a short (τ_1) and long (τ_2) DTC both

in the presence and absence of conjugate preinjection. This difference of diTyr-GdDTPA washout between the two tumor models could be attributed to the variation in morphology of the tumor xenografts originating from two different cell lines due to differences in vascular density [34]. Gli36ΔEGFR tumors showed a more heterogeneous structure with a distinct interface (margin) and core region of the tumor [17]. In contrast, U87ΔEGFR tumors appeared more homogeneous without any clear distinction between the tumor interface and core regions. This may be attributable to a more homogenous tumor blood supply of this aggressive tumor that showed characteristic multiple infiltrations of tumor cell appearing as microdeposits beyond the visible tumor margin (Fig. 6). Different washout kinetics would also be expected if U87ΔEGFR tumors have a larger extracellular accessible compartment than Gli36ΔEGFR tumors.

Furthermore, a comparison of the whole tumor DTCs on Day 2 (τ_1 and τ_2) measured in Gli36ΔEGFR tumors and U87ΔEGFR tumors indicating the retention of the paramagnetic substrate, reveals a similarity in the accumulation of targeted enzyme pair in both tumor models. The slower washout kinetics of the paramagnetic products of enzymatic reaction may offer an alternative diagnostic signature and enable increasing the time window for contrast enhanced tumor imaging irrespective of the tumor type.

Conclusions

a) the lack of complete internalization of enzyme-linked conjugates of EGFRvIII-targeted EMD72000 antibody F(ab')$_2$ fragments in U87ΔEGFR cells suggests the feasibility of MR receptor imaging using a low molecular mass paramagnetic substrate diTyr-GdDTPA as a contrast generating component; b) the conjugates reach orthotopic U87ΔEGFR tumors after the IV administration as demonstrated using radionuclide imaging; c) the washout of diTyr-GdDTPA as measured from DTCs is lengthened following F(ab')$_2$-enzyme conjugates administration *in vivo*, suggesting retention of diTyr-GdDTPA at the sites of EGFRvIII overexpressing cells in the tumors; d) both the differences in elimination kinetics and the presence of specific enhancement patterns after the elimination of free diTyr-GdDTPA provide signatures for tracking the expression of cell surface receptor. MR signal amplification following tumor pre-targeted labeling may aid in earlier and more accurate cancer diagnosis.

Acknowledgments

This work was supported by 5RO1AG034901-03 and 5R01EB000858 grants to AB. We are grateful to Jamie O'Callaghan and Dr. Shaokuan Zheng for assistance with several technical aspects of this work. We are grateful to Dr. Mary Mazzanti for editing the text.

References

1. Weller M, Stupp R, Hegi M, Wick W. Individualized targeted therapy for glioblastoma: Fact or fiction? Cancer J. 2012; 18:40–44. [PubMed: 22290256]
2. Zalatimo O, Zoccoli CM, Patel A, Weston CL, Glantz M. Impact of genetic targets on primary brain tumor therapy: What's ready for prime time? Adv Exp Med Biol. 2013; 779:267–289. [PubMed: 23288644]
3. Murat A, Migliavacca E, Gorlia T, et al. Stem cell-related "Self-renewal" Signature and high epidermal growth factor receptor expression associated with resistance to concomitant chemoradiotherapy in glioblastoma. J Clin Oncol. 2008; 26:3015–3024. [PubMed: 18565887]
4. Chung I, Akita R, Vandlen R, et al. Spatial control of egf receptor activation by reversible dimerization on living cells. Nature. 2010; 464:783–787. [PubMed: 20208517]
5. Ekstrand AJ, Longo N, Hamid ML, et al. Functional characterization of an egf receptor with a truncated extracellular domain expressed in glioblastomas with egfr gene amplification. Oncogene. 1994; 9:2313–2320. [PubMed: 8036013]

6. Nishikawa R, Ji XD, Harmon RC, et al. A mutant epidermal growth factor receptor common in human glioma confers enhanced tumorigenicity. Proc Natl Acad Sci U S A. 1994; 91:7727–7731. [PubMed: 8052651]
7. Shinojima N, Tada K, Shiraishi S, et al. Prognostic value of epidermal growth factor receptor in patients with glioblastoma multiforme. Cancer Res. 2003; 63:6962–6970. [PubMed: 14583498]
8. Hu J, Jo M, Cavenee WK, et al. Crosstalk between the urokinase-type plasminogen activator receptor and egf receptor variant iii supports survival and growth of glioblastoma cells. Proc Natl Acad Sci U S A. 2011; 108:15984–15989. [PubMed: 21896743]
9. Reist CJ, Batra SK, Pegram CN, Bigner DD, Zalutsky MR. In vitro and in vivo behavior of radiolabeled chimeric anti-egfrviii monoclonal antibody: Comparison with its murine parent. Nucl Med Biol. 1997; 24:639–647. [PubMed: 9352535]
10. Mishima K, Johns TG, Luwor RB, et al. Growth suppression of intracranial xenografted glioblastomas overexpressing mutant epidermal growth factor receptors by systemic administration of monoclonal antibody (mAb) 806, a novel monoclonal antibody directed to the receptor. Cancer Res. 2001; 61:5349–5354. [PubMed: 11454673]
11. Johns TG, Adams TE, Cochran JR, et al. Identification of the epitope for the epidermal growth factor receptor-specific monoclonal antibody 806 reveals that it preferentially recognizes an untethered form of the receptor. J Biol Chem. 2004; 279:30375–30384. [PubMed: 15075331]
12. Takasu S, Takahashi T, Okamoto S, et al. Radioimmunoscintigraphy of intracranial glioma xenograft with a technetium-99m-labeled mouse monoclonal antibody specifically recognizing type III mutant epidermal growth factor receptor. J Neurooncol. 2003; 63:247–256. [PubMed: 12892230]
13. Ciardiello F. Epidermal growth factor receptor inhibitors in cancer treatment. Future Oncol. 2005; 1:221–234. [PubMed: 16555994]
14. Wagner TD, Yang GY. Cetuximab: Its use in combination with radiation therapy and chemo-therapy in the multimodality treatment of head and neck cancer. Recent Pat Anticancer Drug Discov. 2008; 3:76–83. [PubMed: 18537749]
15. Weber J, McCormack PL. Panitumumab: In metastatic colorectal cancer with wild-type kras. BioDrugs. 2008; 22:403–411. [PubMed: 18998757]
16. Kamat V, Donaldson JM, Kari C, et al. Enhanced egfr inhibition and distinct epitope recognition by egfr antagonistic mAbs c225 and 425. Cancer Biol Ther. 2008; 7:726–733. [PubMed: 18424917]
17. Shazeeb MS, Sotak CH, DeLeo M 3rd, Bogdanov A Jr. Targeted signal-amplifying enzymes enhance mri of egfr expression in an orthotopic model of human glioma. Cancer Res. 2011; 71:2230–2239. [PubMed: 21245103]
18. Bogdanov AJ, Matuszewski L, Bremer C, Petrovsky A, Weissleder R. Oligomerization of paramagnetic substrates results in signal amplification and can be used for mr imaging of molecualr targets. Mol Imaging. 2002; 1:16–23. [PubMed: 12920857]
19. Querol M, Bennett DG, Sotak C, Kang HW, Bogdanov A Jr. A paramagnetic contrast agent for detecting tyrosinase activity. ChemBioChem. 2007; 8:1637–1641. [PubMed: 17694521]
20. Bogdanov A Jr. Kang HW, Querol M, Pretorius PH, Yudina A. Synthesis and testing of a binary catalytic system for imaging of signal amplification in vivo. Bioconjug Chem. 2007; 18:1123–1130. [PubMed: 17508710]
21. Bogdanov, AJ.; Shazeeb, MS.; Gupta, S. Humanized anti-EGFR antibody fragment/dual enzyme system assists in mr imaging of the receptor deletion variant expression in vivo. The 2012 World Molecular Imaging Congress; Dublin, IR: Springer; 2012. p. S1576
22. Hnatowich DJ, Qu T, Chang F, et al. Labeling peptides with technetium-99m using a bifunctional chelator of a n-hydroxysuccinimide ester of mercaptoacetyltriglycine. J Nucl Med. 1998; 39:56–64. [PubMed: 9443739]
23. Rasband, W. ImageJ. Health USNIo. , editor. Bethesda, Maryland, USA: 1997. http://rsb.info.nih.gov/ij/
24. van Dongen GA, Visser GW, Lub-de Hooge MN, de Vries EG, Perk LR. Immuno-PET: A navigator in monoclonal antibody development and applications. The Oncologist. 2007; 12:1379–1389. [PubMed: 18165614]

25. Sharkey RM, Rossi EA, McBride WJ, Chang CH, Goldenberg DM. Recombinant bispecific monoclonal antibodies prepared by the dock-and-lock strategy for pretargeted radioimmunotherapy. Semin Nucl Med. 2010; 40:190–203. [PubMed: 20350628]
26. McCabe KE, Liu B, Marks JD, et al. An engineered cysteine-modified diabody for imaging activated leukocyte cell adhesion molecule (alcam)-positive tumors. Mol Imaging Biol. 2012; 14:336–347. [PubMed: 21630083]
27. Stoldt HS, Aftab F, Chinol M, et al. Pretargeting strategies for radioimmunoguided tumour localisation and therapy. Eur J Cancer. 1997; 33:186–192. [PubMed: 9135486]
28. Boerman OC, van Schaijk FG, Oyen WJ, Corstens FH. Pretargeted radioimmunotherapy of cancer: Progress step by step. J Nucl Med. 2003; 44:400–411. [PubMed: 12621007]
29. Goldenberg DM, Chang CH, Rossi EA, et al. Pretargeted molecular imaging and radioimmunotherapy. Theranostics. 2012; 2:523–540. [PubMed: 22737190]
30. Artemov D, Mori N, Ravi R, Bhujwalla ZM. Magnetic resonance molecular imaging of the her-2/neu receptor. Cancer Res. 2003; 63:2723–2727. [PubMed: 12782573]
31. Zeglis BM, Mohindra P, Weissmann GI, et al. Modular strategy for the construction of radiometalated antibodies for positron emission tomography based on inverse electron demand diels-alder click chemistry. Bioconjug Chem. 2011; 22:2048–2059. [PubMed: 21877749]
32. Bogdanov A Jr. Matuszewski L, Bremer C, Petrovsky A, Weissleder R. Oligomerization of paramagnetic substrates results in signal amplification and can be used for mr imaging of molecular targets. Mol Imaging. 2002; 1:16–23. [PubMed: 12920857]
33. Schmiedel J, Blaukat A, Li S, Knochel T, Ferguson KM. Matuzumab binding to EGFR prevents the conformational rearrangement required for dimerization. Cancer Cell. 2008; 13:365–373. [PubMed: 18394559]
34. Packard SD, Mandeville JB, Ichikawa T, et al. Functional response of tumor vasculature to Paco2: Determination of total and microvascular blood volume by MRI. Neoplasia. 2003; 5:330–338. [PubMed: 14511404]

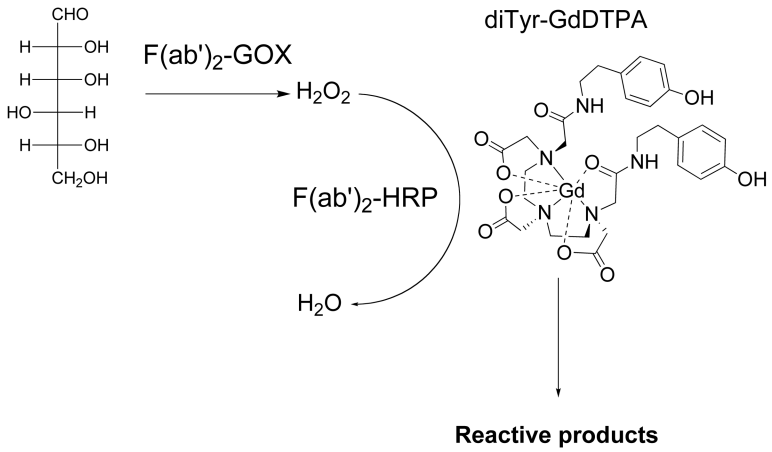

Figure 1.
Reaction of diTyr-GdDTPA with enzyme pair (GOX/HRP) conjugated to F(ab')$_2$ fragments of humanized anti-EGFRvIII monoclonal antibody.

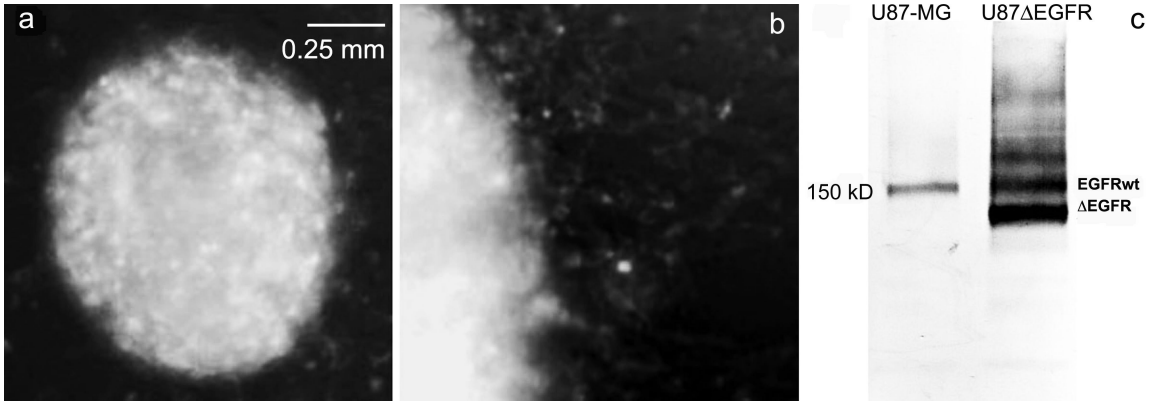

Figure 2.

Expression of truncated EGFR variant in U87ΔEGFR cells. (**a**) Fluorescence microscopy of U87ΔEGFR spheroid; (**b**) Migration of EGFRvIII-positive cells on a plastic surface; (**c**) The expression of EGF receptor and its variants by the parent U87-MG glioblastoma cells and in U87ΔEGFR variant revealed by immunoblotting of cell membrane fraction using anti-EGFR antibody.

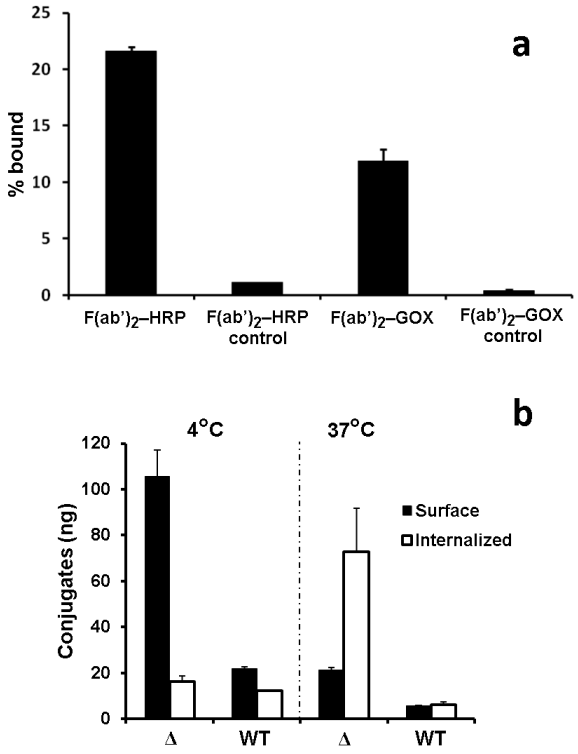

Figure 3.

In vitro specificity and internalization of radiolabeled EMD72000 mAb F(ab')$_2$ conjugates. (**a**) Cell binding assay showing specificity of radiolabeled EMD72000 mAb F(ab')$_2$ conjugates for U87ΔEGFR. Control samples contained a 10-fold molar excess of unlabeled conjugates. (**b**) U87ΔEGFR cell-surface binding (black bars) and internalization (white bars) of the conjugate mixture at the optimized HRP/GOX ratio (1:2, w/w) in U87ΔEGFR (Δ) and U87-MG (WT) cells at 4°C and 37°C.

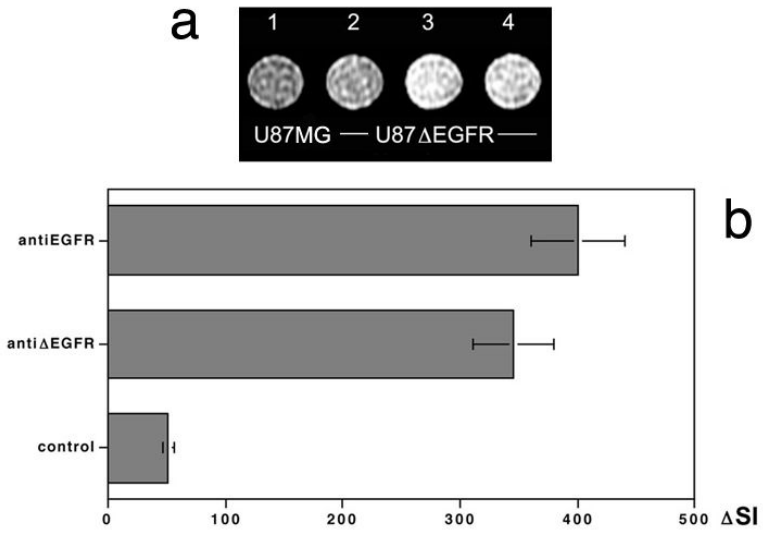

Figure 4.

MR imaging of enzyme-mediated EGFR specific signal amplification effect. (**a**) T1W spin-echo (TE 11 ms/TR 200 ms) images of cell pellets at 1.5T. (1) U87-MG cells incubated with anti-EGFRvIII EMD72000 mAb F(ab')$_2$ conjugates of HRP and GOX (1 μg/ml total mAb) followed by 0.15 mM of diTyr-GdDTPA substrate in 0.5 mM glucose/PBS, (2) control pellet of U87ΔEGFR cells incubated in the presence of 0.15 mM diTyr-GdDTPA only, (3) pellet of U87ΔEGFR cells incubated with anti-EGFRvIII C225 mAb F(ab')$_2$ conjugates followed by 0.15 mM diTyr-GdDTPA, (4) U87ΔEGFR cell pellet incubated with anti-EGFRvIII EMD72000 mAb F(ab')$_2$ conjugates followed by 0.15 mM diTyr-GdDTPA. (**b**) Quantification of MR signal-intensity change in images shown in (a) after subtracting the background signal of U87ΔEGFR cells.

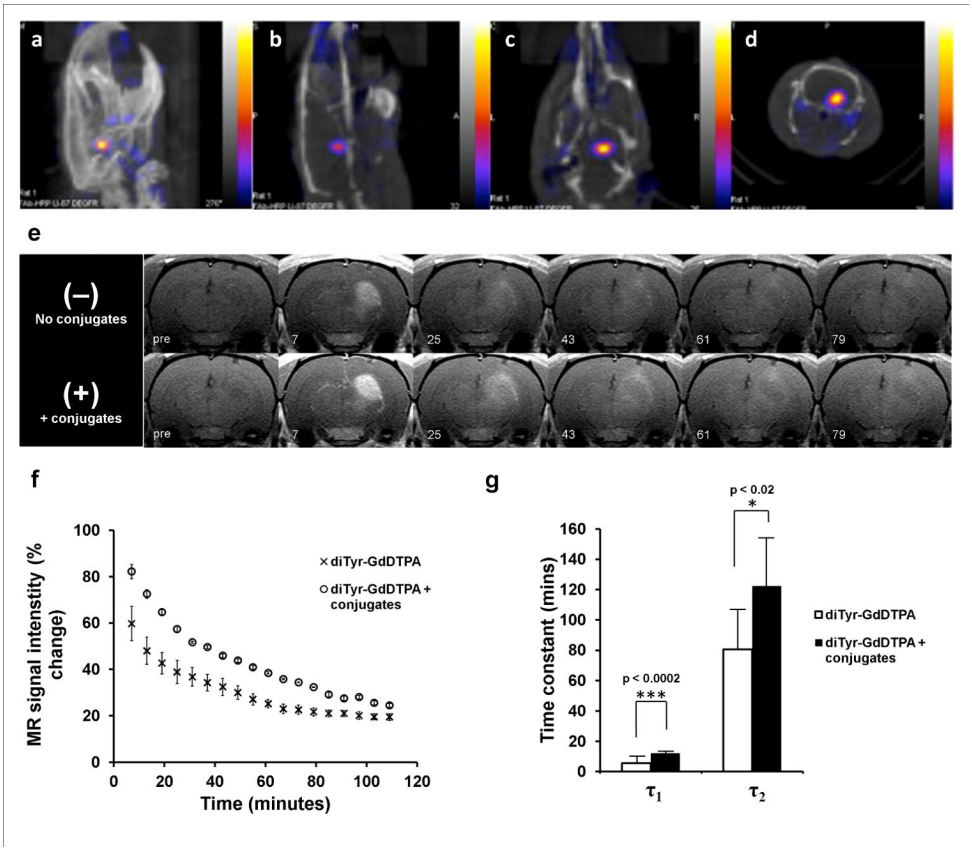

Figure 5.

SPECT/CT and 3T MR imaging of U87ΔEGFR human glioma xenografts in the rat brain. SPECT/CT images are shown with: (**a**) maximum intensity pixel (MIP) projection images, and (**b**) sagittal, (**c**) coronal, and (**d**) axial projections of an athymic rat brain bearing a U87ΔEGFR xenograft. Color scale corresponds to measured radioactivity reflecting the accumulation of ^{99m}Tc-labeled mAb F(ab')$_2$ conjugates in U87ΔEGFR xenografted tumors. (**e**) Sequential T1-weighted rat brain images depicting enhancement as a function of time after injection of diTyr-GdDTPA. Top row – temporal washout of diTyr-GdDTPA with no conjugate pre-injection (Day 1). Bottom row – washout of diTyr-GdDTPA following pre-treatment with EMD72000 mAb F(ab')$_2$ conjugates (Day 2) in the same slice for the same animal. Time intervals (in minutes) after the injection of diTyr-GdDTPA are shown below. (**f**) Normalized signal intensities measured in the whole volume of U87ΔEGFR tumor slices from a representative animal prior to (crosses) and post injection of conjugates (circles) as a function of time post-diTyr-GdDTPA substrate injection. The signal intensities are normalized as a percent change relative to the pre-contrast image. (**g**) Decay time constants (DTCs) measured from normalized T1-weighted signal intensities of diTyr-GdDTPA washout in the tumor region of animals with U87ΔEGFR tumors (n=5) prior to injection of conjugates (white bars), or after pre-injection of EMD72000 mAb F(ab')$_2$ conjugates (black bars). Tumor ROI regions of animals on both days with and without pre-injection of EMD72000 mAb F(ab')$_2$ conjugates exhibited biexponential signal decay. Both DTCs (τ_1 and τ_2) were significantly greater in the presence of EMD72000 mAb F(ab')$_2$ conjugates compared to only diTyr-GdDTPA substrate injection.

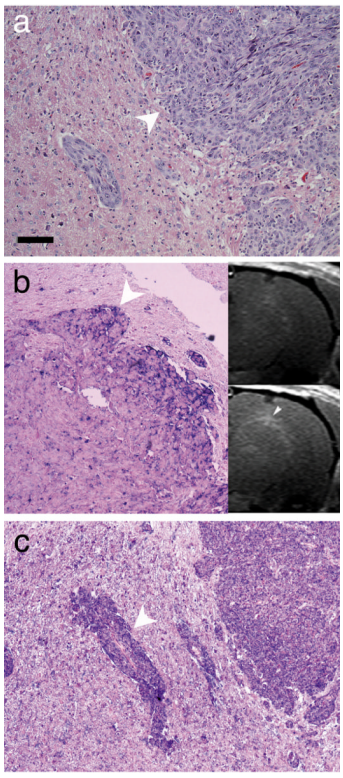

Figure 6.

Histology of U87ΔEGFR xenograft. (**a**) H&E staining of tumor/normal brain interface (the tumor infiltrative margin is shown with an arrowhead). (**b**) Anti-EGFRvIII AP-staining showing overexpression of the receptor at the tumor margin. The inset shows the matching MRI slice before (upper image) and after the consecutive injection of EMD72000 mAb $F(ab')_2$-GOX and $F(ab')_2$-HRP conjugates followed by diTyr-GdDTPA (lower image) at the 43 min time point. An arrowhead shows the regional enhancement that corresponds to the area of receptor overexpression. (**c**) Immunohistochemistry showing HRP distribution in the same tumor demonstrated by using anti-HRP mAb after the injection of anti-EGFRvIII HRP conjugate. Note the overexpression detected at the margin of tumor micro infiltrate, shown with an arrowhead. Nuclei were counterstained using Nuclear Fast Red. Bar = 50 μm.

Table 1

Kinetic elimination constants for diTyr-GdDTPA in the U87ΔEGFR tumor region with and without pre-injection of EGFRvIII targeted F(ab')$_2$-enzyme conjugates.

	Decay time constants (min)	
	τ_1 (min) *a)*	τ_2 (min) *a)*
Control (No preinjection of conjugates) Day 1	6 ± 3	81 ± 28
Experiment (With pre-injection of EMD72000 (anti-EGFRvIII) F(ab')$_2$ conjugates) Day 2	12 ± 0.4	122 ± 35
P values	P < 0.0002 *b)*	P < 0.02 *c)*

a) Based on χ^2 analysis using an *F* test, a biexponential function was found to best model the signal-intensity-decay curves for the U87ΔEGFR tumor regions that were pre-injected with anti-EGFRvIII conjugates (Day 2) and that were not pre-injected with conjugates (Day 1);

P values correspond to significant differences between decay time constants (τ values) in:

b) between τ_1 values in the tumor region with and without F(ab')$_2$ conjugate pre-injection;

c) between τ_2 values in the tumor region with and without F(ab')$_2$ conjugate pre-injection.